ACS APPLIED MATERIALS & INTERFACES

Research Article

www.acsami.org

Semitransparent Polymer Solar Cells with 5% Power Conversion Efficiency Using Photonic Crystal Reflector

Wenjuan Yu,[†] Liang Shen,*[,†] Ping Shen,[‡] Yongbing Long,[§] Hongwei Sun,[†] Weiyou Chen,[†] and Shengping Ruan*[,‡]

[†]State Key Laboratory on Integrated Optoelectronics and [‡]College of Electronic Science and Engineering, Jilin University, 2699 Qianjin Street, Changchun 130012, People's Republic of China

[§]School of Applied Physics and Materials, Institute of Thin Film and Nanomaterials, WuYi University, No. 22, Dongchen Cun, Jiangmen 529020, People's Republic of China

ABSTRACT: Efficient semitransparent polymer solar cells (ST-PSCs) have been fabricated with one-dimensional photonic crystals (1DPCs) as a high reflector. The 1DPCs are composed of several pairs of WO_3 (65.8 nm)/LiF (95.5 nm). By optimizing the pairs of WO_3/LiF, 1DPCs can reflect the light back into the ST-PSCs due to the photonic band gap, when the high reflectance range of 1DPCs is matched with absorption spectrum of the active layer. ST-PSCs with 8 pairs of 1DPC exhibit an attractive performance. The short-circuit current density (J_{sc}) and power conversion efficiency (PCE), respectively, reach to 9.76 mA/cm^2 and 5.16% compared to 8.12 mA/cm^2 and 4.24% of the reference ST-PSCs without 1DPCs. A maximum enhancement of 20.2% in J_{sc} is obtained and the PCE increases by ~21.7%. This approach provides a simple, fascinating and promising method to realize the highly efficient ST-PSCs toward applications.

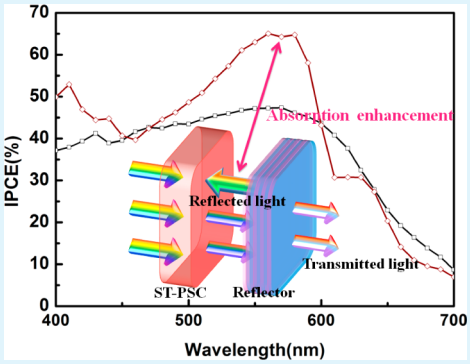

KEYWORDS: *semitransparent, low-bandgap polymer solar cells, transmittance, reflectance, one-dimensional photonic crystals, distributed Bragg reflector*

1. INTRODUCTION

In past decade, polymer solar cells (PSCs) have attracted enormous research interest due to the potential of easy fabrication, low-cost production and promising flexibility.[1−3] Along with the remarkable progress in designing low bandgap polymers, the power conversion efficiency (PCE) of a single junction PSC has reached to 9.2%.[4] Recently, a PCE of 10.6% has been achieved in a tandem structure, making this clean solar energy convertor to play an important role in future renewable energy manufacture.[5,6] However, in order to achieve commercialization and large-scale production, PSCs need to have not only high performance but also unique properties.[7−10] So, semitransparent PSCs (ST-PSCs),[11] stretchable PSCs,[12] and photonic color filters integrated PSCs appear and show fascinating properties.[13] Especially, ST-PSCs are incorporated with transparent cathodes and anodes.[14−16] It means that ST-PSCs can utilize a part of light to generate electricity, and transmit another part of light to illuminate. It can be integrated with the energy-harvesting window, automobile windshields, foldable curtains, and other architectural applications. The semitransparent properties can appropriately satisfy the requirement of the inherent transparent property and power generation simultaneously.[17−21] There are two important factors for ST-PSCs, transparency and PCE. The PCE of ST-PSCs is relatively lower than conventional PSCs,[22−25] because there is a contradiction between the efficiency and transparency of ST-PSCs. To maintain the total transmittance of ST-PSCs, a thin active layer and a transparent top electrode are indispensable. However, the thin active layer and the transparent top electrode results in the insufficient absorption in the active layer because the thickness of top electrode is not enough to support a strong mirror reflection. It can only absorb a part of incident light and the rest runs across the devices. The loss of light absorption leads to a lower efficiency for ST-PSCs owing to device structure. In early studies, poly(3-hexylthiophene) (P3HT) and [6,6]-phenyl C_{61} butyric acid methyl ester ($PC_{60}BM$) were frequently used as the active layer materials for ST-PSCs and the PCE was generally below 2.5%.[26−28] Obviously, this PCE of ST-PSCs is not good enough for commercialization. However, further improvement of the PSCs based on P3HT: $PC_{60}BM$ is limited by the narrow absorption range and the relatively small energy difference between the highest occupied molecular orbital (HOMO) of P3HT and the lowest unoccupied molecular orbital (LUMO) of the fullerene acceptor, which results in a low open-circuit voltage (V_{oc}) about 0.6 V.[29,30] In order to pursue high performance ST-PSCs, studies are devoted to the development of low bandgap polymers with strong absorption.[31−34] Another promising strategy is to employ a tandem structure ST-PSCs.

Received: October 22, 2013
Accepted: December 17, 2013
Published: December 17, 2013

C. Chen et al. reported a tandem ST-PSCs with highest PCE of 7.3% and average transmittance (AVT) of 30%.[15]

Herein, we report a highly efficient ST-PSC with one-dimensional photonic crystals (1DPCs) based on poly[*N*-9″-hepta-decanyl-2,7-carbazole-*alt*-5,5-(4′,7′-di-2-thienyl-2′,1′,3′-benzothiadiazole)] (PCDTBT): [6,6]-phenyl C71-butyric acid methyl ester ($PC_{70}BM$). The ST-PSC exhibits both high PCE (5.16%) and excellent transmittance (74% at 682 nm). The AVT (400−800 nm) is about 29.3% which is satisfied with the ST-PSCs' commercialization requirement, while the AVT of reference ST-PSC is about 28.4%. The device structure is glass/indium tin oxides (ITO)/titanium oxide (TiO_2)/PCDTBT:$PC_{70}BM$/tungsten oxide (WO_3)/silver (Ag)/[WO_3/ lithium fluoride (LiF)]^N (Figure 1).

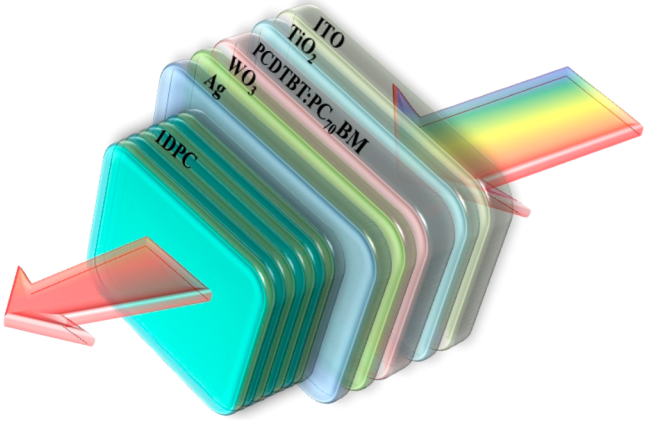

Figure 1. Device architecture of ST-PSC with 8 pairs of 1DPC (Device E).

PCDTBT, which has a deeper HOMO level than P3HT, was synthesized by M. Leclerc et al. in 2007. The deeper HOMO level can notably increase the V_{oc} of PSCs.[35−37] In the initial report of PCDTBT, they demonstrated a PSCs PCE of 3.6% with a higher V_{oc} approaching 0.9 V.[35] Subsequently, Bazan's group improved the efficiency of PSCs based on PCDTBT to 6.5% via incorporation of a conjugated polyelectrolyte interlayer.[38] In the paper, the higher J_{sc} and favorable transmittance of ST-PSCs are obtained from 1DPCs as distributed Bragg reflector (DBR). It can reflect the light back into the active layer with the photonic bandgap and increase the light absorption. In Figure 2a, the absorption range of the PCDTBT:$PC_{70}BM$ film is 400−650 nm. Here, the 1DPCs' reflectance center is set as 550 nm and 1DPC with 8 pairs of WO_3/LiF shows a high reflectance by approaching to 100% in 480−650 nm, which exactly matched with the absorption range from 500 to 620 nm of the PCDTBT:$PC_{70}BM$. The light (500−620 nm) will be reflected back into the active layer and reabsorbed again. For the rest, there is a high transmittance as a result of the passband of the 1DPCs. High PCE and high AVT meet the accordance with ST-PSCs' application requirements. Especially, this is a unilateral ST-PSC, which can produce strong photovoltaic effect only when incident light illuminate from ITO side. When illuminated from top electrode, the 1DPC as distributed reflectors will reflect the light back to the air.

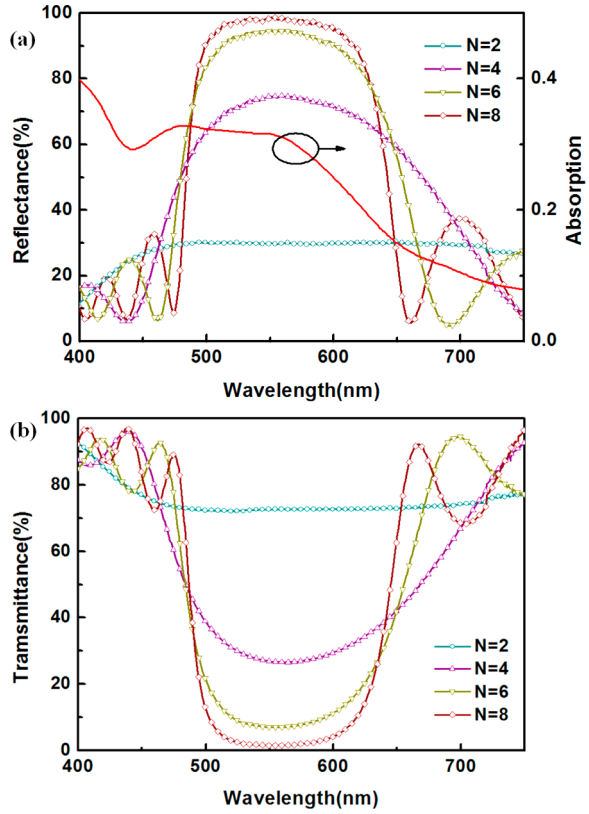

Figure 2. (a) Reflectance spectra of 1DPCs and the absorption spectrum of PCDTBT:$PC_{70}BM$. (b) Transmittance spectra of 1DPCs.

2. EXPERIMENTAL SECTION

2.1. Fabrication and Characterization of 1DPCs. The 1DPCs are composed of *N* pairs of WO_3 (Sinopharm Chemical Reagent Co. Ltd.) and LiF (Luminescence Technology Corp.) layers. *N* is the number of repeated period and equal to 2, 4, 6, and 8. *N* pairs of WO_3 (65.8 nm)/LiF (95.5 nm) were alternately evaporated under a high vacuum (5×10^{-4} Pa) without disrupting the vacuum. The deposition rate was about 1 nm/s, which was monitored by a quartz-oscillating thickness monitor (ULVAC, CRTM-9000). The transmittance and reflectance spectra of 1DPCs were measured by means of an ultraviolet/visible spectrometer (UV1700, Shimadzu) with a quartz glass substrate.

2.2. Fabrication and Characterization of ST-PSCs with 1DPCs. The preparation of devices is described in the following. The reference device structure is glass/ITO(150 nm)/TiO_2(25 nm)/PCDTBT:$PC_{70}BM$ (80 nm)/WO_3(10 nm)/Ag(15 nm) (device A). The structure of 1DPCs-based ST-PSCs is glass/ITO(150 nm)/TiO_2 (25 nm)/PCDTBT: $PC_{70}BM$ (80 nm)/WO_3(10 nm)/Ag(15 nm)/[WO_3/LiF]^N (devices B−E). Device E is shown in Figure 1. In the fabrication, the ITO-conducting glass substrate (a sheet resistance of 15Ω/sq) was first precleaned by acetone, ethanol and deionized water for 15 min respectively followed by treatment with oxygen plasma for 10 min. Anatase TiO_2 thin films were prepared as described in our previous papers.[39] PCDTBT (Lumtec Corp) was dissolved in 1,2-dichlorobenzene to produce 7 mg/mL solution, followed by blending with $PC_{70}BM$ (Lumtec Corp) in 1:4 weight ratio. The blend was stirred for 72 h in glovebox filled with argon. The PCDTBT: $PC_{70}BM$ active layer with a thickness of 80 nm was prepared by spin coating on top of TiO_2 film surface at 2000 rpm for 30 s. The samples were annealed at ∼70 °C for 25 min in glovebox. Then, the devices were evaporated of 10 nm WO_3 and 15 nm Ag in sequence under a high vacuum (5×10^{-4} Pa) without disrupting the vacuum. The Ag top electrode was evaporated through a shadow mask to define the active area of the devices. The device dimension was 0.064 cm^2. The deposition rate was about 0.3 nm/s, which was monitored by a quartz-

dx.doi.org/10.1021/am405274z | ACS Appl. Mater. Interfaces 2014, 6, 599−605

oscillating thickness monitor (ULVAC, CRTM-9000). For the semitransparent devices with 1DPCs, N pairs of WO_3 (65.8 nm)/LiF (95.5 nm) were alternately evaporated under a high vacuum (5×10^{-4} Pa) without disrupting the vacuum. The deposition rate was about 1 nm/s. N is equal to 2, 4, 6, and 8. Correspondingly, the devices were named by device B, device C, device D, and device E.

$J-V$ characteristics were measured with a computer-programmed Keithley 2601 source meter under AM1.5G solar illuminations with an Oriel 300 W solar simulator intensity of 100 mW/cm^2 (about one sun). The light intensity was measured with a photometer (International light, IL1400) corrected by a standard silicon solar cell. The absorption, reflectance and transmittance spectra were measured by an ultraviolet/visible spectrometer (UV1700, Shimadzu). IPCE was measured with a Crowntech QTest Station 1000AD. The transmittance spectra of Device E under different incident angles are tested by Spectroscopic Ellipsometer (M-2000UI, J. A. Woollam. Co. Inc.).

3. EXPERIMENTAL AND SIMULATION RESULTS AND DISSCUSSION

3.1. Design and Characterization of the 1DPCs. 1DPCs have been known as a multilayer reflector and have a refractive index that is periodic in one-dimensional.[40] Photons with energies lying in the photonic band gap cannot propagate through the 1DPCs. The alternate thickness and refraction index is d_1, d_2, n_1, and n_2 respectively.[41] For a quarter-wave stack in the periodic structure, there is a fixed relationships between n_1, n_2, d_1, and d_2.[42] The optical path of every layer is exactly 1/4 of the center wavelength λ_0. The relationship formulation is as follows:

$$n_1 d_1 = n_2 d_2 = \frac{\lambda_0}{4} = \frac{\pi c}{2\omega_0} \quad (1)$$

where c is the vacuum speed of light. When eq 1 is met, the reflected light from every interface has an identical phase and then the constructive interference starts up. For these quarter-wave stack 1DPCs, a high reflectance approaching to 100% around center wavelength λ_0 is expected.

To achieve an appropriate reflector on the ST-PSCs, we use the 1DPCs as the DBR. According to the active layer absorption range, the central position of the DBR should be located at 550 mn which is the absorption peak of PCDTBT:$PC_{70}BM$. Then, the ST-PSCs can absorb the incident light by twice or more times and result in improvement in efficiency. We select WO_3 with a high refractive index and LiF with a low refractive index as the periodicity repeated unit components. Assuming the pair number N is infinite, the position of the photonic band gap can be adjusted continuously by the thickness of WO_3 and LiF. Here, the refractive index of WO_3 and LiF is 2.08 (n_1) and 1.44 (n_2), respectively. According to eq 1, the thickness of WO_3 and LiF can be calculated, which is 65.8 and 95.5 nm, respectively.

To study the effect of pairs number N on reflectance and transmittance of 1DPCs, the reflectance and transmittance spectra of the 1DPCs with different pairs of N (2, 4, 6, 8) (Figure 2) was tested. In 500−620 nm, the reflectance of the 1DPCs increases gradually (Figure 2a) and the corresponding transmittance decreases as the N increases (Figure 2b). With further increased N, a high reflectance of approaching to 100% and a low transmittance of near 0% in 500−620 nm is gained. Consequently, the maximum pairs of the N = 8 is chosen to achieve enough high reflectance. There is a match between the absorption spectrum of the active layer and the reflectance spectra of the 1DPCs. The light (500−620 nm) has to stay in the device, because it almost cannot transmit in 1DPCs. This resident light causes absorption by twice or more times based on a changed light distribution. But the rest light can transmit in 8 pairs of 1DPC successfully due to the narrow forbidden photonic bandgap of 1DPCs.

3.2. Device Performance Characteristics. The $J-V$ characteristics of devices based on different N are shown in Figure 3a under 100 mW/cm^2 simulated AM1.5G in ambient air. For comparison, the reference device A without 1DPCs was also tested. Relatively, device A has a lower circuit current density (J_{sc}) of 8.12 mA/cm^2, an open-circuit voltage (V_{oc}) of 0.85 V, a fill factor (FF) of 61.4%, and an overall PCE of 4.24%. Device E has a J_{sc} of 9.76 mA/cm^2, a V_{oc} of 0.85 V, a FF of 62.2%, and an overall PCE of 5.16% shown in Table 1. It can be

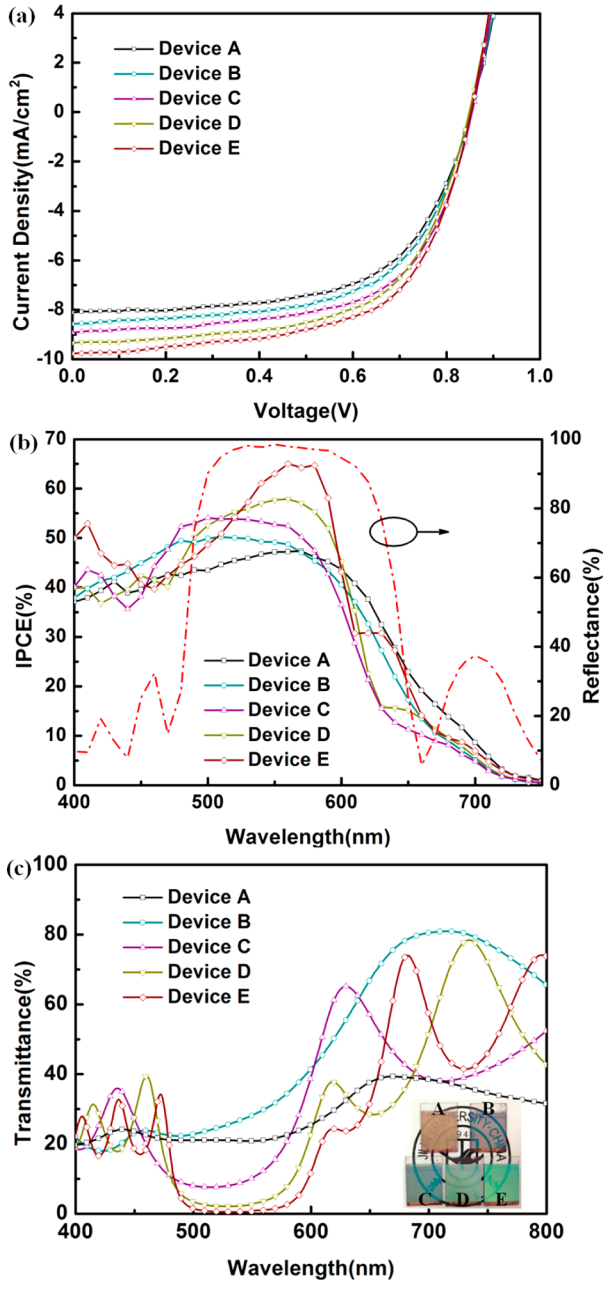

Figure 3. (a) $J-V$ characteristics of devices A−E, under 100 mW/cm^2 simulated AM1.5G in ambient air. (b) IPCE characteristics of devices A−E and reflectance spectrum of 8 pairs of 1DPC. (c) Transmittance spectra of devices A−E.

dx.doi.org/10.1021/am405274z | ACS Appl. Mater. Interfaces 2014, 6, 599−605

Table 1. Detailed Performance Parameters of Devices A–E, under 100 mW/cm^2 Simulated AM1.5G in Ambient Air

device	J_{sc} (mA/cm^2)	V_{oc} (V)	FF (%)	PCE (%)
A	8.12	0.85	61.4	4.24
B	8.57	0.85	61.4	4.47
C	8.93	0.85	62.6	4.75
D	9.34	0.85	61.6	4.89
E	9.76	0.85	62.2	5.16

clearly observed that the FF and V_{oc} of the five devices are almost same, and it clearly shows that FF and V_{oc} are independent of the DBR. Meanwhile, there is a significant increment in the J_{sc}. With the increase of (WO_3/LiF) pairs of N, the J_{sc} is improved gradually. A maximum enhancement of 20.2% in J_{sc} is obtained while N = 8 and the PCE increases about 21.7%.

To confirm the improvement in the J_{sc}, the IPCE tests for devices A–E are shown in Figure 3b. The IPCE spectrum of the device E is found to be significantly enhanced in a broad wavelength range of 500–620 nm when compared with device A. The IPCE improvement should be attributed to high reflectance of the 1DPCs within the photonic bandgap (500–620 nm). Correspondingly, the improvement of device performance is owing to the high reflectance of 1DPC. For the reference device, the active layer can absorb a part incident light and the unabsorbed light transmits through the thin Ag semitransparent top electrode. But for Device E, the unabsorbed light runs across the semitransparent Ag anode and reaches the 1DPCs, which is capped on the Ag anode. The 1DPCs can reflect all the light within the photonic bandgap of 500–620 nm back into the active layer for reabsorption, which will enhance the utilization of the light within the wavelength range of 500–620 nm.

Furthermore, the total device transmittance spectra of devices A–E are presented in Figure 3c, in which the corresponding photos of devices A–E are inserted. The AVTs in 400–800 nm of device A and device E are 28.4% and 29.3%, respectively. The highest transmittance of 1DPC is 74% at 682 nm. This shows that the moderate transmittance in 650–800 nm holds the transparency of device E. Specially, in 500–620 nm, the transmittance of device A is higher than that of device E due to the high reflectance of 8 pairs of 1DPC in this region. So, the light in 500–620 nm, which belongs to green light wavelength range, cannot transmit through device E. Therefore, the photo of device E appears green. However, device A still can transmit a part of light in this available wavelength range. It results in the loss on the photocurrent and the efficiency in device A. Generally speaking, device E has a high PCE about 5.16% attributed to secondary absorption of the available light (500–620 nm) based on a high AVT.

3.3. Theoretical Simulations. To further investigate the improvement of J_{sc} resulting from the effect of the 1DPCs, the field intensity across the middle of the PCDTBT:PC_{70}BM active layer, the optical electric field distribution, the absorption spectra and $J_{sc\text{-}max}$ were calculated based on the transfer matrix method (TMM).[43,44] All layers are assumed planar and isotropy in the simulations.

In Figure 4a, the field intensities are shown across the middle of the PCDTBT:PC_{70}BM active layer for the device A and device E, respectively. The field intensity of device E is much higher than that of device A below 620 nm. In this wavelength range, the AM1.5G normalized photon density (AM1.5G NPD) is significantly higher. So, the significant field intensity enhancement improves the overall photocurrent.

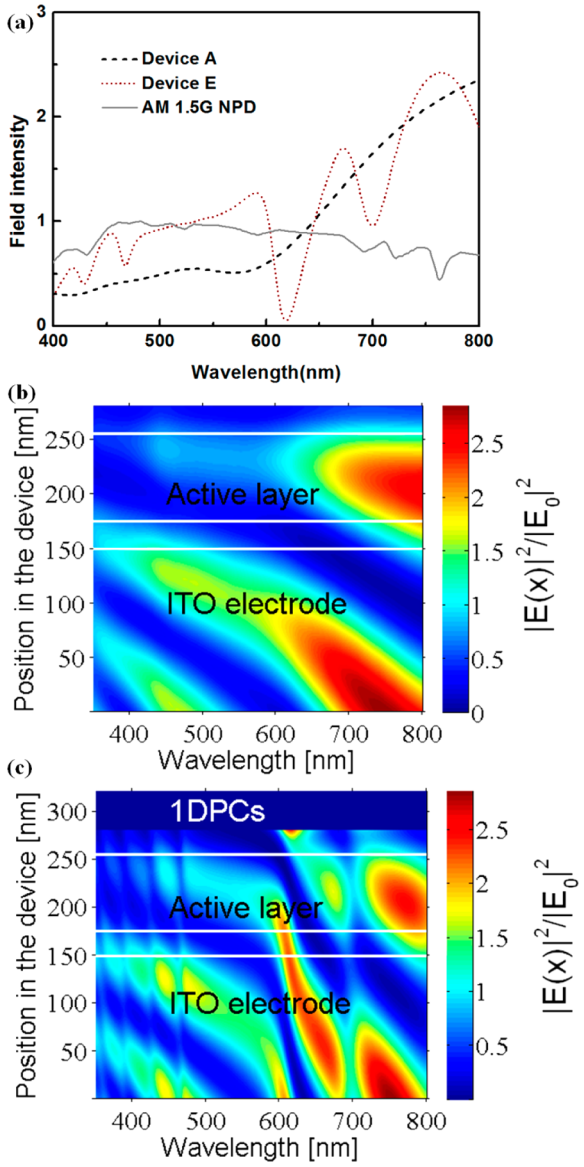

Figure 4. (a) Field intensity in the middle of the photoactive region for device A and device E, and the AM1.5G normalized photon density (NPD). (b) Distribution of normalized modulus square of the optical electric field of device A. (c) Distribution of normalized modulus square of the optical electric field of device *E*. $|E_0|^2$ is the modulus square of the optical electric field for the incident light.

To further investigate the J_{sc} enhancement in device E, the optical electric field distributions ($|E(x)|^2$) in device A and device E are calculated and shown in Figure 4b and c. In the calculation, the absorption in the active layer is neglected. Obviously, the optical electric field in the active layer of device E is much higher in wavelength 500–620 nm than that of device A. This higher optical field is caused by the high reflectance of 1DPCs. Since the reflectance of 1DPCs strengthens in the wavelength range of 500–620 nm as the pair number (N) of WO_3/LiF increases, the IPCE spectra of the ST-PSCs are gradually enhanced and then an improvement in J_{sc} and PCE can be expected.

The changes of optical electric field distribution in devices cause an enhanced optical absorption in the active layer. So, in

dx.doi.org/10.1021/am405274z | ACS Appl. Mater. Interfaces 2014, 6, 599–605

order to clarify the absorption enhancement, the absorption spectra of devices A and E are calculated in Figure 5a. There is

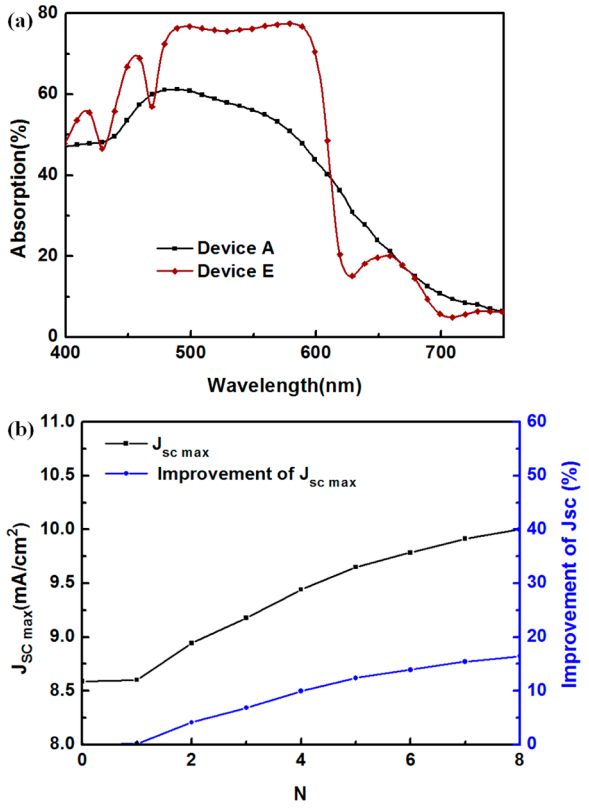

Figure 5. (a) Simulated absorption spectra of devices A and E. (b) $J_{sc\text{-}max}$ as a function of the pair of 1DPCs and the improvement in $J_{sc\text{-}max}$ as a function of the pair of 1DPCs.

a dramatic difference of absorption spectra for the PSC devices with or without 8 pairs of 1DPC. For device E with 1DPCs, the absorption is much higher than that of device A within the wavelength range of 500−620 nm. The peak value of the absorption spectrum of device E is about 0.78 from 500 to 620 nm, in which the shape is similar to the reflectance spectrum of 8 pairs of 1DPC. The improvement occurs because the light reflected from the 1DPCs is absorbed by the active layer again, which leads to a distinct electric field distribution and eventually results in distinct absorption spectra of devices A and E.

Above all, the increased absorption can induce a higher J_{sc}. This drastically enhanced J_{sc} is also confirmed by calculation. Assuming that all absorbed photons are converted into collected charges (i.e., the internal quantum efficiency (IQE) equals to one) and the devices are illuminated with AM1.5G at 100 mW/cm^2, the upper limit to photocurrent generation can be calculated as $J_{sc\text{-}max}$.[45,46] The $J_{sc\text{-}max}$ is calculated as a function of the pairs of 1DPCs in Figure 5b. When N is increased from 2 to 8, $J_{sc\text{-}max}$ is enhanced gradually. For device A (N = 0) and device E (N = 8), the $J_{sc\text{-}max}$ values are about 8.5 and 10.0 mA/cm^2. It indicated device E can achieve higher $J_{sc\text{-}max}$ based on reflector 1DPCs. In order to further compare $J_{sc\text{-}max}$ of devices with different pairs of 1DPCs, the improvement of $J_{sc\text{-}max}$ is calculated by dividing the difference of $J_{sc\text{-}max}$ of semitransparent devices with 1DPCs (N = 1−8) and device A by the $J_{sc\text{-}max}$ of device A. As shown in Figure 5b, the improvement of $J_{sc\text{-}max}$ gradually increased. For device E, the improvement of $J_{sc\text{-}max}$ is about 16.4%.

As is well-known, the 1DPC structure possesses angle dependent optical properties.[47−52] The photonic bandgap comes from the interference of Bragg scattering in the periodical dielectric structure. As the incident angle varies, the interference process inside the 1DPC is changed. Therefore, to study the angle dependency relationship of ST-PSCs, the properties of device E with DBR under different incident angles were tested. In Figure 6a, the J_{sc}'s of device E

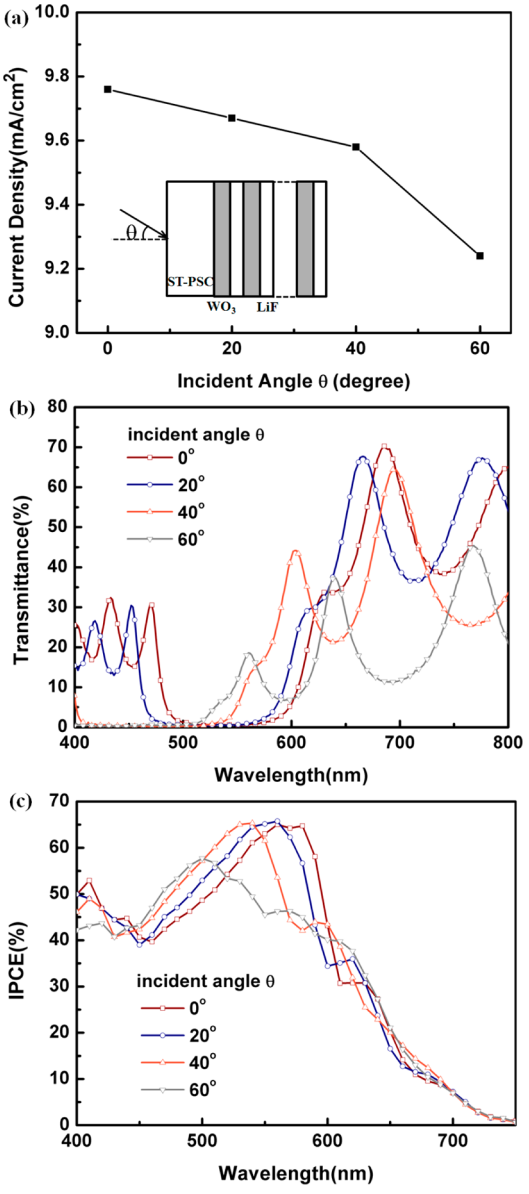

Figure 6. (a) J_{sc} of device E under different incident angles. (b) Transmittance spectra of device E as a function of different incident angles. (c) IPCE characteristics of device E under different incident angles.

corresponding to different incident angles θ (0°, 20°, 40°, and 60°) are 9.76, 9.67, 9.58, and 9.24 mA/cm^2, respectively. θ, which is shown at the bottom of Figure 6a, is the angle between incident light and surface normal of 1DPC. It can be seen that the J_{sc} slightly decreased as the incident angle increased between 0° and 40°. When the angle was equal to 60°, the J_{sc}

dx.doi.org/10.1021/am405274z | ACS Appl. Mater. Interfaces 2014, 6, 599−605

decreased obviously. The V_{oc} and FF of these tested results almost remain unchanged because the angle cannot change the transportation of charge carrier.[53,54] Figure 6b shows the transmittance spectra of device E under different incident angles, which are tested via spectroscopic ellipsometer. It can be seen that the low transmittance region, which corresponds to the photonic band gap of 1DPC, shifts distinctly toward the short wavelength and the width is gradually increased. According to refs 48 and 49, the edges of the directional photonic band gaps will shift to higher frequencies and broaden with the increase of incident angle. It means that the low transmittance region will shift to the lower wavelength because the normalized frequency has a reciprocal relation with wavelength. The theory is in accordance with our experiment results.

To clarify the influence of angular dependence of 1DPC on device E, the IPCE spectra based on various incident angles have been measured and shown in Figure 6c. The IPCE spectra have a blue shift, which is in accordance with the transmittance spectra. When the angle is smaller than 60°, the IPCE spectrum shifts toward the short wavelength equably and the peak values almost remain unchanged. It can be attributed to the fact that the 1DPCs' photonic band gaps still match with the absorption region of PCDTBT:$PC_{70}BM$ (450−650 nm) in this case. However, the IPCE declines dramatically when the angle reaches to 60°. It can be seen that the photonic band gap is shifted below 500 nm as shown in Figure 6b, which results in a mismatch with the absorption region.

4. CONCLUSION

In conclusion, we demonstrate a simple and fascinating method to achieve efficient ST-PSCs by incorporate the 1DPCs as a DBR. The 1DPCs reflector can reflect the part of light which is within the active layer absorption range to improve the device absorption based on a suitable total transmittance. ST-PSCs with 8 pairs of 1DPC exhibit an attractive performance. The J_{sc} and PCE reached 9.76 mA/cm^2 and 5.16%, respectively. The phenomenon mechanism of the enhanced J_{sc} is investigated through experiment and theoretical simulations, which manifest the enhanced absorption induces a higher J_{sc}. Meanwhile, the AVT of ST-PSCs with 8 pairs of 1DPC is 29.3%. At last, the influence of incident angles on properties of ST-PSCs is tested. The device transmittances shift distinctly toward the short wavelength as the angle increases. The IPCE spectra also have a blue shift which is in accordance with the transmittance spectra and the peak values almost remain unchanged when the angle smaller than 60°. This method meets the qualification of applications that integrated onto window panes to enhance the functionality of utilized transparent surfaces.

AUTHOR INFORMATION

Corresponding Authors

*E-mail: shenliang@jlu.edu.cn.
*E-mail: ruansp@jlu.edu.cn.

Notes

The authors declare no competing financial interest.

ACKNOWLEDGMENTS

The authors are grateful to National Natural Science Foundation of China (Grant Nos. 61275035, 61370046), Chinese National Programs for High Technology Research and Development (863 program: 2013AA030902), Doctoral Found of Ministry of Education of China (Grant No. 20110061130004), Project of Science and Technology Development Plan of Jilin Province (Grant Nos. 20110314, 20120324), Scientific Frontier and Interdiscipline Innovative Projects of Jilin University (Grant No. 2013ZY18), the Foundation for Industrial Technology Research and Development Projects of Jiangmen City (Grant No. 2012-156-09), and Natural Science Foundation of Guangdong Province, China (Grant No. S2013010012854) for the support to the work.

REFERENCES

(1) Li, G.; Zhu, R.; Yang, Y. *Nat. Photonics* **2012**, *6*, 153−161.
(2) Lin, H. W.; Chiu, S. W.; Lin, L. Y.; Hung, Z. Y.; Chen, Y. H.; Lin, F.; Wong, K. T. *Adv. Mater.* **2012**, *24*, 2269−2272.
(3) Tromholt, T.; Gevorgyan, S. A.; Jørgensen, M.; Krebs, F. C.; Sylvester-Hvid, K. O. *ACS Appl. Mater. Interfaces* **2009**, *1*, 2768−2777.
(4) He, Z.; Zhong, C.; Su, S.; Xu, M.; Wu, H.; Cao, Y. *Nat. Photonics* **2012**, *6*, 593−597.
(5) You, J.; Chen, C. C.; Hong, Z.; Yoshimura, K.; Ohya, K.; Xu, R.; Ye, S.; Gao, J.; Li, G.; Yang, Y. *Adv. Mater.* **2013**, *25*, 3973−3978.
(6) You, J.; Dou, L.; Yoshimura, K.; Kato, T.; Ohya, K.; Moriarty, T.; Emery, K.; Chen, C.-C.; Gao, J.; Li, G. *Nat. Commum.* **2013**, *4*, 1446−1455.
(7) Taylor, R.; Otanicar, T.; Rosengarten, G. *Light: Sci. Appl.* **2012**, *1*, e34-1−e34-7.
(8) Nakamura, M.; Yang, C.; Zhou, E.; Tajima, K.; Hashimoto, K. *ACS Appl. Mater. Interfaces* **2009**, *1*, 2703−2706.
(9) Beyer, B.; Pfeifer, R.; Zettler, J. K.; Hild, O. R.; Leo, K. *J. Phys. Chem. C* **2013**, *117*, 9537−9542.
(10) Chang, C. Y.; Zuo, L.; Yip, H. L.; Li, Y.; Li, C. Z.; Hsu, C. S.; Cheng, Y. J.; Chen, H.; Jen, A. K. Y. *Adv. Funct. Mater.* **2013**, *23*, 5084−5090.
(11) Shen, L.; Xu, Y.; Meng, F.; Li, F.; Ruan, S.; Chen, W. *Org. Electron.* **2011**, *12*, 1223−1226.
(12) Lipomi, D. J.; Tee, B. C. K.; Vosgueritchian, M.; Bao, Z. *Adv. Mater.* **2011**, *23*, 1771−1775.
(13) Park, H. J.; Xu, T.; Lee, J. Y.; Ledbetter, A.; Guo, L. J. *ACS Nano* **2011**, *5*, 7055−7060.
(14) Tao, C.; Xie, G.; Meng, F.; Ruan, S.; Chen, W. *J. Phys. Chem. C* **2011**, *115*, 12611−12615.
(15) Chen, C.-C.; Dou, L.; Gao, J.; Chang, W.-H.; Li, G.; Yang, Y. *Energy Environ. Sci.* **2013**, *6*, 2714−2720.
(16) Li, F.; Ruan, S.; Xu, Y.; Meng, F.; Wang, J.; Chen, W.; Shen, L. *Sol. Energy Mater. Sol. Cells* **2011**, *95*, 877−880.
(17) Chueh, C. C.; Chien, S. C.; Yip, H. L.; Salinas, J. F.; Li, C. Z.; Chen, K. S.; Chen, F. C.; Chen, W. C.; Jen, A. K. Y. *Adv. Energy Mater.* **2013**, *3*, 417−423.
(18) Yu, W.; Shen, L.; Shen, P.; Meng, F.; Long, Y.; Wang, Y.; Lv, T.; Ruan, S.; Chen, G. *Sol. Energy Mater. Sol. Cells* **2013**, *117*, 198−202.
(19) Tang, Z.; George, Z.; Ma, Z.; Bergqvist, J.; Tvingstedt, K.; Vandewal, K.; Wang, E.; Andersson, L. M.; Andersson, M. R.; Zhang, F. *Adv. Energy Mater.* **2012**, *2*, 1467−1476.
(20) Chen, C.-C.; Dou, L.; Zhu, R.; Chung, C.-H.; Song, T.-B.; Zheng, Y. B.; Hawks, S.; Li, G.; Weiss, P. S.; Yang, Y. *ACS Nano* **2012**, *6*, 7185−7190.
(21) Guo, F.; Zhu, X.; Forberich, K.; Krantz, J.; Stubhan, T.; Salinas, M.; Halik, M.; Spallek, S.; Butz, B.; Spiecker, E. *Adv. Energy Mater.* **2013**, *3*, 1062−1067.
(22) Lin, H.-W.; Chen, Y.-H.; Huang, Z.-Y.; Chen, C.-W.; Lin, L.-Y.; Lin, F.; Wong, K.-T. *Org. Electron.* **2012**, *13*, 1722−1728.
(23) Zhang, D.-D.; Jiang, X.-C.; Wang, R.; Xie, H.-J.; Ma, G.-F.; Ou, Q.-D.; Chen, Y.-L.; Li, Y. Q.; Tang, J. *ACS Appl. Mater. Interfaces* **2013**, *5*, 10185−10190.
(24) Krebs, F. C. *Sol. Energy Mater. Sol. Cells* **2009**, *93*, 394−412.
(25) Hau, S. K.; Yip, H.-L.; Zou, J.; Jen, A. K.-Y. *Org. Electron.* **2009**, *10*, 1401−1407.

(26) Amb, C. M.; Craig, M. R.; Koldemir, U.; Subbiah, J.; Choudhury, K. R.; Gevorgyan, S. A.; Jørgensen, M.; Krebs, F. C.; So, F.; Reynolds, J. R. *ACS Appl. Mater. Interfaces* **2012**, *4*, 1847−1853.
(27) Li, W.; Lee, T.; Oh, S. J.; Kagan, C. R. *ACS Appl. Mater. Interfaces* **2011**, *3*, 3874−3883.
(28) Yu, W.; Shen, L.; Ruan, S.; Meng, F.; Wang, J.; Zhang, E.; Chen, W. *Sol. Energy Mater. Sol. Cells* **2012**, *98*, 212−215.
(29) Kim, J. Y.; Noh, S.; Nam, Y. M.; Kim, J. Y.; Roh, J.; Park, M.; Amsden, J. J.; Yoon, D. Y.; Lee, C.; Jo, W. H. *ACS Appl. Mater. Interfaces* **2011**, *3*, 4279−4285.
(30) Sista, S.; Hong, Z.; Chen, L.-M.; Yang, Y. *Energy Environ. Sci.* **2011**, *4*, 1606−1620.
(31) Zhang, Y.; Zou, J.; Cheuh, C.-C.; Yip, H.-L.; Jen, A. K.-Y. *Macromolecules* **2012**, *45*, 5427−5435.
(32) Yang, T.; Wang, M.; Duan, C.; Hu, X.; Huang, L.; Peng, J.; Huang, F.; Gong, X. *Energy Environ. Sci.* **2012**, *5*, 8208−8214.
(33) He, Z.; Zhong, C.; Huang, X.; Wong, W. Y.; Wu, H.; Chen, L.; Su, S.; Cao, Y. *Adv. Mater.* **2011**, *23*, 4636−4643.
(34) Li, X.; Choy, W. C.; Huo, L.; Xie, F.; Sha, W. E.; Ding, B.; Guo, X.; Li, Y.; Hou, J.; You, J. *Adv. Mater.* **2012**, *24*, 3046−3052.
(35) Blouin, N.; Michaud, A.; Leclerc, M. *Adv. Mater.* **2007**, *19*, 2295−2300.
(36) Zilberberg, K.; Behrendt, A.; Kraft, M.; Scherf, U.; Riedl, T. *Org. Electron.* **2013**, *14*, 951−957.
(37) Park, S. H.; Roy, A.; Beaupré, S.; Cho, S.; Coates, N.; Moon, J. S.; Moses, D.; Leclerc, M.; Lee, K.; Heeger, A. J. *Nat. Photonics* **2009**, *3*, 297−302.
(38) Seo, J. H.; Gutacker, A.; Sun, Y.; Wu, H.; Huang, F.; Cao, Y.; Scherf, U.; Heeger, A. J.; Bazan, G. C. *J. Am. Chem. Soc.* **2011**, *133*, 8416−8419.
(39) Shen, L.; Zhu, G.; Guo, W.; Tao, C.; Zhang, X.; Liu, C.; Chen, W.; Ruan, S.; Zhong, Z. *Appl. Phys. Lett.* **2008**, *92*, 073307.
(40) Foresi, J.; Villeneuve, P. R.; Ferrera, J.; Thoen, E.; Steinmeyer, G.; Fan, S.; Joannopoulos, J.; Kimerling, L.; Smith, H. I.; Ippen, E. *Nature* **1997**, *390*, 143−145.
(41) Winn, J. N.; Fink, Y.; Fan, S.; Joannopoulos, J. *Opt. Lett.* **1998**, *23*, 1573−1575.
(42) Scalora, M.; Flynn, R.; Reinhardt, S.; Fork, R.; Bloemer, M.; Tocci, M.; Bowden, C.; Ledbetter, H.; Bendickson, J.; Dowling, J. *Phys. Rev. E* **1996**, *54*, R1078.
(43) Sergeant, N. P.; Hadipour, A.; Niesen, B.; Cheyns, D.; Heremans, P.; Peumans, P.; Rand, B. P. *Adv. Mater.* **2012**, *24*, 728−732.
(44) Pettersson, L. A.; Roman, L. S.; Inganas, O. *J. Appl. Phys.* **1999**, *86*, 487−496.
(45) Long, Y. *Sol. Energy Mater. Sol. Cells* **2010**, *94*, 744−749.
(46) Eerenstein, W.; Slooff, L.; Veenstra, S.; Kroon, J. *Thin Solid Films* **2008**, *516*, 7188−7192.
(47) Lee, H.-Y.; Yao, T. *J. Appl. Phys.* **2003**, *93*, 819−830.
(48) Li-Gang, W.; Nian-Hua, L.; Qiang, L.; Shi-Yao, Z. *Phys. Rev. E* **2004**, *70*, 016601-1−016601-12.
(49) Wang, X.; Hu, X.; Li, Y.; Jia, W.; Xu, C.; Liu, X.; Zi, J. *Appl. Phys. Lett.* **2002**, *80*, 4291−4293.
(50) Dardano, P.; Gagliardi, M.; Rendina, I.; Cabrini, S.; Mocella, V. *Light: Sci. Appl.* **2012**, *1*, e42-1−e42-5.
(51) Wu, J.; Horsley, S.; Artoni, M.; Rocca, G. *Light: Sci. Appl.* **2013**, *2*, e54-1−e54-5.
(52) Talghader, J.; Gawarikar, A.; Shea, R. *Light: Sci. Appl.* **2012**, *1*, e24-1−e24-5.
(53) Riede, M.; Uhrich, C.; Widmer, J.; Timmreck, R.; Wynands, D.; Schwartz, G.; Gnehr, W. M.; Hildebrandt, D.; Weiss, A.; Hwang, J. *Adv. Funct. Mater.* **2011**, *21*, 3019−3028.
(54) Tvingstedt, K.; Andersson, V.; Zhang, F.; Inganas, O. *Appl. Phys. Lett.* **2007**, *91*, 123514−123514-3.